Registration of computed tomography images of a lung infected with COVID-19 based in the new meta-heuristic algorithm HPSGWO

Hedifa Dida [1] · Fella Charif [1] · Abderrazak Benchabane [1]

Abstract

Computed tomography (CT) helps the radiologist in the rapid and correct detection of a person infected with the coronavirus disease 2019 (COVID-19), and this by showing the presence of the ground-glass opacity in the lung of with the virus. Tracking the evolution of the spread of the ground-glass opacity (GGO) in the lung of the person infected with the virus needs to study more than one image in different times. The various CT images must be registration to identify the evolution of the ground glass in the lung and to facilitate the study and identification of the virus. Due to the process of registration images is essentially an improvement problem, we present in this paper a new HPSGWO algorithm for registration CT images of a lung infected with the COVID-19. This algorithm is a hybridization of the two algorithms Particle swarm optimization (PSO) and Grey wolf optimizer (GWO). The simulation results obtained after applying the algorithm to the test images show that the proposed approach achieved high-precision and robust registration compared to other methods such as GWO, PSO, Firefly Algorithm (FA), and Crow Searcha Algorithms (CSA).

Keywords COVID-19 · Computed tomography · Ground-glass opacity · Particle swarm optimization · Grey wolf optimizer · Image registration

1 Introduction

In the medical field, the radiologist relies on the detection of many diseases on different medical imaging methods, as it provides information that helps him identify early and diagnose accurately. Computed tomography (CT) is one of the methods that has been used to diagnose many tumors, as this method provides information on solid tissue of organs [6].

✉ Hedifa Dida
   dida.hedifa@univ–ouargla.dz

[1] Faculty of New Information and Communication Technologies, Department of Electronics and Telecommunications, Kasdi Merbah University, Ouargla, Algeria

This method was used to detect many modern diseases, especially those caused by the coronavirus disease 2019 (COVID-19) in recent days.

COVID-19 is a deadly virus that has recently emerged in the Chinese town of Wuhan, has spread around the world, and has left many victims. Symptoms of this virus include coughing, fever, and shortness of breath, as well as other symptoms, that is, its symptoms are not specific, which makes early detection of people with this virus very difficult [24, 41]. The doctors relied on early detection of this virus on the results of a computed tomography which, showed ground-glass opacity (GGO) even for infected persons and showed no symptoms [26]. Figure 1 shows the CT results of a case infected with COVID-19, as it clearly shows the distribution of GGO on both sides of the lung. The images of the lung infected with the virus are taken by means of computing tomography at different time periods to understand the development of GGO [14], so knowing all the areas where these opacities appeared are needed study each image individually. Therefore, the radiologist needs a technique that helps him to maximize the quality of CT image to detect and the presence of ground-glass opacities in the lung and track its development before and after appearing the symptoms of infection with COVID-19. Medical image registration is an essential step that has been widely used to facilitate the diagnostic process for radiologists.

In general, image registration can be defined as the process of matching two or more images, source of these images can be different sensors, different point of view, or captured at various times [17]. This process is based on the calculation of a spatial transformation function between two images to be superimposed on the optimum of their resemblance criteria. The image registration process is based on three main components: a transformation model, a similarity metric, and an optimization method [16]. Similarity metrics that are used in this field are based on intensity difference, cross-correlation, and mutual information (MI). However, the MI metric is the most used in multimodal image registration. The search strategy to find the best transformation parameters in the image registration process is mainly based on the optimization method. Many methods of improvement were used in the process of registratering images, such as Downhill Simplex, conjugate gradient descent, and Levenberg-Marquardt method [16].

Recently, the use of meta-heuristic algorithms have witnessed a wide range of activity for their effectiveness in finding solutions to many optimization problems that are difficult to solve by exact optimization methods, due to properties, such as high dimensionality, multimodality, epistasis (parameter interaction), and non-differentiability [18]. These algorithms rely on continuous iteration in search of solutions to improve problems as the iteration process stops
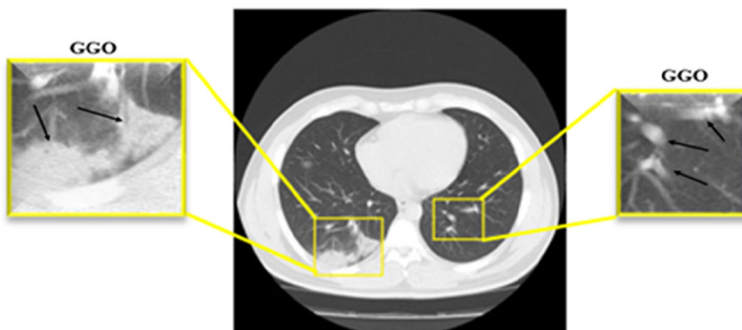
Fig. 1 CT scan results of a virus-infected lung showing the presence of GGO on both sides of the lung

when a stopping criterion is satisfied [22]. There are many meta-heuristic algorithms that differ according to the way they search for solutions among these methods, we have Particle swarm optimization (PSO) [35], Grey wolf optimizer (GWO) [16], Firefly Algorithm (FA) [38], Crow Searcha Algorithm (CSA) [8]. Despite the success of these algorithms in many optimization processes, their solutions remain relative and do not reach the required optimization.

To achieve better registration, in this paper, we present the HPSGWO algorithm for recording images of lungs infected with COVID-19 using CT methods by maximizing the value of the mutual information. The algorithm HPSGWO is a hybridization of the two algorithms, PSO and GWO, thus combining the advantages of the two algorithms in the optimization process.

The remainder of this paper is organized as follows: The second section explains the related work. The third section presents the proposed method. The third section describes the proposed method (HPSGWO algorithm), and PSO, GWO, FA, and CSA algorithms. In the fourth section, simulation results are presented and a comparison study between algorithms is discussed, and then discussed. In the fifth and final section, a conclusion is drawn form this work.

2 Related work

The field of image analysis is wide and varies according to the method used in image processing, as most of them aim to reduce noise, provide a clearer image, and contains the required amount of information. Several methods have been adopted in the field of image processing, some of which are based on the convolution network [40], including those based on iterative Structure-adaptive Fuzzy Estimation [11], as well as based on an artifact suppressed dictionary learning [10]. This work is about medical image registration Especially the CT images of the lung of a person with COVID-19. The main of this work is to obtain a more detailed image with an acceptable amount of information to facilitate the diagnosis of infection with this virus.

2.1 Medical image registration process

Generally, the image registration process is described as aligning two or more images and combining them to the best similarity criterion. This process is an essential pillar in many applications of image analysis in general and medical imaging in particular [19]. Image registration is based on three components: a transformation which relates the target (sensed or moving) image Is and source (reference or fixed) image Ir, a similarity measure S which measures the similarity between target and source image, and an optimization algorithm which determines the optimal transformation parameters as a function of the similarity measure [13]. Figure 1 presents the steps required in the image registration process.

In the image registration process, the sensed image undergoes a series of transformations to correspond the reference image depending on a similarity metric. The process of changing the parameters of the transformation continues until the two images are optimal similar. The optimal transformation parameters T of the two images undergoing the registration process can be obtained by maximizing the similarity metric S, the following equation illustrates this process [29]:

$$\hat{T} = \arg \max_{T} S[I_r(x, y), I_s(T(x, y))] \tag{1}$$

Where (x, y) is the coordinates of the image.

2.1.1 Geometric transformation of images

Establishing one-to-one correspondence between pixels or boxels needs to relate the target plane or volume to the reference by means of the transformation T [29]. The transformation model is responsible for determining the type of geometrical transformation to be applied for the registration. The transformation models can be rigid (universal) or non-rigid (flexible). Rigid transformation models are characterized by no distortions or small deformations if any, and the entire image is transformed uniformly, whereas non-rigid models use large and complex deformations [36]. In this paper, our study is limited to applying rigid transformation, which is contains a translations along x and y axes t_x, t_y, and rotation θ. This transformation is popular because in many common medical images the rigid body constraint leads to a good approximation. Furthermore, it has relatively few parameters to be determined and it can be defined as [5]:

$$M = \begin{bmatrix} \cos(\theta) & \sin(\theta) & t_x \\ -\sin(\theta) & \cos(\theta) & t_y \\ 0 & 0 & 1 \end{bmatrix} \tag{2}$$

2.1.2 Similarity measure

Mutual information of image intensities is a new matching criterion that features robust and completely automatic registration of multi-modal images without prior segmentation [20]. These advantages make the proposed mutual information method suitable for many different applications involving CT images. For two images A and B of individual entropy and joint entropy, the Mutual information between these two images can be calculated as follows:

$$MI(A, B) = H(A) + H(B) - H(A, B) \tag{3}$$

Where:

$$H(A) = -\sum_a P_A(a) \log_2 P_A(a), \tag{4}$$

$$H(A, B) = -\sum_{a,b} P_{A,B}(a, b) \log_2 P_{A,B}(a, b), \tag{5}$$

Where $P_A(a)$ and $P_{A, B}(a, \ b)$ are the marginal distributions of probability that can be viewed as a combined PDF projection onto the axes corresponding to the intensities in images A and B, respectively [15].

2.1.3 Optimizer

The optimization is an essential component and very important step in the image registration process. The role of optimization is to search the geometric transformation that is applied to the scene to make it as similar as possible to the model, in other words [13], find the optimum

transformation parameters required for aligning the images. There are several optimization methods that differ according to the algorithms used. According to the nature of the algorithm, the optimization algorithms can be categorized into three categories: deterministic algorithms, stochastic algorithms and hybrid algorithms which is a mixture of deterministic and stochastic algorithms. Figure 2 illustrates the categories of this classification [27].

3 Proposed method

In our proposed method is based on the use of meta-heuristic algorithms to record CT images that were taken at different times (Figs. 3 and 4).

3.1 Particle swarm optimization

Particle swarm optimization (PSO) is a population-based meta-heuristic optimization method. Was proposed by Eberhart and Kennedy in 1995, which is a stochastic optimization technique that simulates the animal's social behavior when searching for food, including insects, herds, birds and fishes, and is therefore dependent mainly on swarm [34]. The algorithm configuration is related to a group of particles, where each of the particles represents a candidate solution to a problem and has the following three main attributes: the position in the search space $X_i(t)$, the current velocity $V_i(t)$ and the best position ever found by the particle during the search process $X_i^*(t)$ [9]. The velocity of each particle is adjusted by the following equations:

$$V_i(t+1) = wV_i(t) + C_1R_1\left[X_i^*(t) - X_i(t)\right] + C_2R_2\left[X_g^*(t) - X_i(t)\right] \tag{6}$$

Here:

$$w = \left(w_{max} - w_{min}\right)\left(\frac{T_{max} - 1}{T_{max}}\right) \tag{7}$$

Where $X_i^*(t)$ is the best position of each particle which represents the private best objective (fitness) value so far obtained, and $X_g^*(t)$ is the global best particle which denotes the best position among all particles in the population. ω represents the inertia weight which is used to
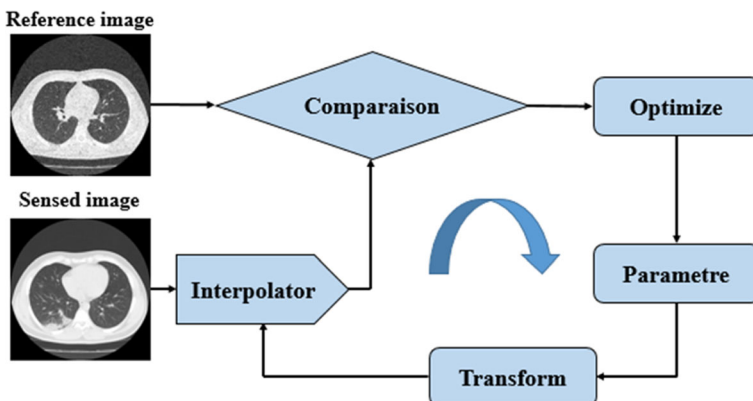
Fig. 2 Block diagram of image registration process
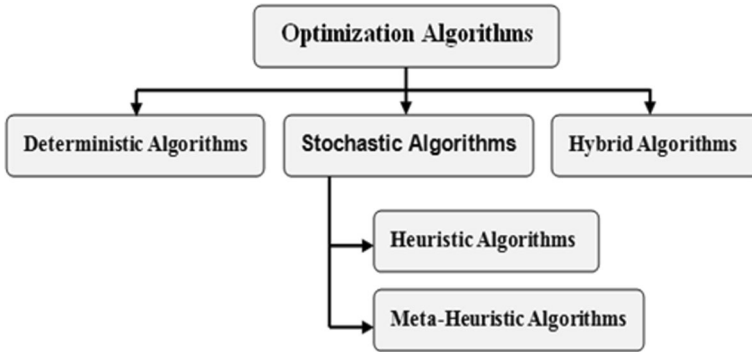
Fig. 3 The general classification of the optimization algorithms

maintain the particle, C_1 and C_2 represent cognition learning and social learning factor, respectively, and R_1, R_2 are the uniformly generated random numbers in the range of [0, 1].

The process of moved each particle by adding speed to the current position is as follows:

$$X_i(t+1) = X_i(t) + V_i(t+1) \qquad (8)$$

Where $X_i(t + 1)$ is the new position, and $V_i(t + 1)$ indicates the new velocity.

3.2 Grey wolf optimizer

The gray wolf algorithm is an algorithm inspired by the gray wolves' living system in the wild, which belong to a canadian family. These wolves prefer to live in groups, the group size is each averaging between 5 and 15, and follow a strict dominant social hierarchy [32]. Gray wolves are divided into three groups, each of which has a different role to play. Among the set of possible solutions, the best solution appears in alpha wolves. This can be shown by the following equation:

$$\vec{X}(t+1) = \vec{X}_p(t) - \vec{A}.\vec{D} \qquad (9)$$

Where $\vec{X}$ and $\vec{X}_p$ the grey wolf and target position, respectively, t is the number of iteration and $\vec{D}$ is distance vector calculated as:

$$\vec{D} = \left| \vec{C} .\vec{X}_p - \vec{X}(t) \right| \qquad (10)$$

(a) CT-I1   (b) CT-I2   (c) CT-I3   (d) CT-I4
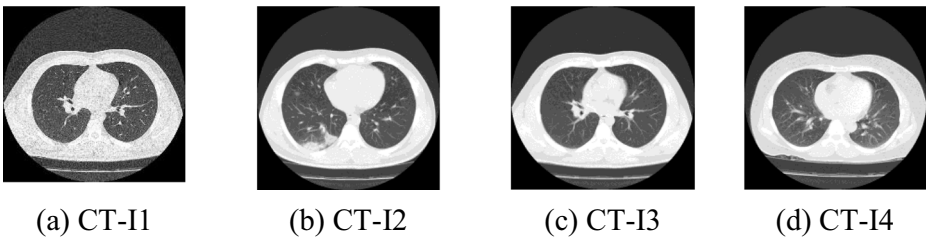
Fig. 4 Real 2D images of the lungs infected with COVID-19. (a) CT-I1, (b) CT-I2, (c) CT-I3, (d) CT-I4

Springer

Here, and $\overrightarrow{C}$ are the coefficient vectors. These coefficient vectors are shown in eqs. (11) and (12), respectively.

$$\overrightarrow{A} = 2.k.\overrightarrow{p}_1 - k \tag{11}$$

$$\overrightarrow{C} = 2.\overrightarrow{p}_2 \tag{12}$$

Where $K = 2 - t\left(\frac{t}{T_{max}}\right)$ is decreased from 2 to 0 linearly through the number of iterations, T_{max} is total number of iterations and $\overrightarrow{p}_1$, $\overrightarrow{p}_2$ are two random vectors between [0, 1]. The alpha is responsible for directed the fishing pattern of the wolves. Beta and Delta are also involved in fishing. Thus, the first three best solutions are chosen to be the hunting wolves, and their current positions can update all wolves' positions. The formulas in this regard are as follows:

$$\begin{cases} \overrightarrow{D}_\alpha = \left|\overrightarrow{C}_1.\overrightarrow{X}_\alpha - \overrightarrow{X}\right| \\ \overrightarrow{D}_\beta = \left|\overrightarrow{C}_2.\overrightarrow{X}_\beta - \overrightarrow{X}\right| \\ \overrightarrow{D}_\delta = \left|\overrightarrow{C}_3.\overrightarrow{X}_\delta - \overrightarrow{X}\right| \end{cases} \tag{13}$$

After computing the difference vectors $\overrightarrow{D}_\alpha$, $\overrightarrow{D}_\beta$, and $\overrightarrow{D}_\delta$, as well as the updated states for (t + 1), the iteration can be computed as follows:

$$\begin{cases} \overrightarrow{X}_1 = \overrightarrow{X}_\alpha - \overrightarrow{A}_1 \overrightarrow{D}_\alpha \\ \overrightarrow{X}_2 = \overrightarrow{X}_\beta - \overrightarrow{A}_2 \overrightarrow{D}_\beta \\ \overrightarrow{X}_2 = \overrightarrow{X}_\delta - \overrightarrow{A}_3 \overrightarrow{D}_\delta \end{cases} \tag{14}$$

$$\overrightarrow{X}(t+1) = \frac{\overrightarrow{X}_1 + \overrightarrow{X}_2 + \overrightarrow{X}_3}{3} \tag{15}$$

Where $\overrightarrow{A}_1$, $\overrightarrow{A}_2$, and $\overrightarrow{A}_3$ are the random vectors,

3.3 Firefly algorithm

Firefly Algorithm (FA) is a randomization-based optimization algorithm to find solutions inspired by the nature of fireflies and their ability to glow [37]. This algorithm is described by by the rhythmic flashes that fireflies send in order to warn of the possibility and the presence of prey or to bring in other fireflies easily. Least brighter fireflies move in the direction of the other brighter fireflies, that is, the greater the distance between the fireflies, the attractiveness decreased between thefireflies, which leads to random movement of the fireflies [1]. Equation 9 illustrates the variation of the firefly's light attractive coefficient β with the distance r between the heifers [2].

$$\beta = \beta_0 e^{-\gamma r^2} \tag{16}$$

Where β_0 is the attractiveness at zero distance (r = 0) and normally set to 1. And γ is the light absorption coefficient.

3.4 Crow searchal algorithm

The CSA algorithm was inspired from crows behavior in obtaining their food. Crows depend on stealing to obtain their food, as they follow other birds and take food after those birds leave their hiding place [31]. The behavior of the crows prompted researchers to create an algorithm that mimics this behavior, called it crow search algorithm. Equation 3 illustrates the formula in which crows change their position while observing the awareness of other birds [23]:

$$X_i^{t+1} = \begin{cases} X_i^t + r_i \times fl_i^t \times \left| m_i^t - X_i^t \right| & r_i \geq AP_i^t \\ a \; random \; position & otherwise \end{cases} \tag{17}$$

Where AP_i^t represents the awareness of the crow j. If the victim bird knows that the crow is following it, he will try to take the crow to a random location. For each crow i, a crow j is selected randomly to update the position of crow i [23].

3.5 Hybrid PSO-GWO (HPSGWO)

Grey wolf optimizer (GWO) and Particle swarm optimization (PSO) algorithms each have features that determine their importance in overcoming various optimization problems [28, 30]. While each of the aforementioned algorithms has flaws in the way it searches for solutions to a problem.

3.5.1 PSO algorithm

Despite the advantages of the PSO algorithm, such as the robustness in solving many optimization problems, not to mention the simplicity and ease of implementation, it often falls into the minimum solutions when it is subjected to severe restrictions [30].

3.5.2 GWO algorithm

The gray wolf algorithm maintains a balance between exploration and exploitation and often avoids being trapped locally. It is also characterized by speed and accuracy of results. Despite all this, it remains limited compared to PSO in overcoming many problems.

This approach was inferred by GWO using wolves 'positions α, β, and δ in determining the solution as shown in Eq. 2 with wolves' position updated on the one hand, and by PSO using *gbest*, *pbest*, and inertia (w) as shown in Eq. 7, as it provides him with information about tracking and discovering the best location of particles from another side. The hybrid approach used the orientation characteristic used by GWO with the prior knowledge provided by PSO by *gbest*, *pbest* and inertia (w) to obtain an algorithm that has broad ability to overcome the problems of image registration, accuracy in results and speed in performance. This hybrid approach can be described by increasing the GWO performance. Equation 18 shows the positions customized to the wolf:

$$\vec{X}_{wolf}(t+1) = \frac{\vec{X}_1 + \vec{X}_2 + \vec{X}_3}{3} \tag{18}$$

Here the mean of the best three can be calculated and it represents the the gbest of the proposed algorithm. The pbest and inertia (w) are predicted in the same way as the traditional PSO algorithm. The estimation of the positions of the new GWO algorithm related to the PSO algorithm is shown in the following equation:

$$\vec{X}_i^{t+1} = w\vec{X}_i + C_1.R_1\left(\overrightarrow{pbest_i}\right) + C_2(1-R_2)\left(\overrightarrow{gbest}\right) \tag{19}$$

Here:

$$gbest = \frac{\vec{X}_1 + \vec{X}_2 + \vec{X}_3}{3} \tag{20}$$

Here, R_1 and R_2 are the random variables are bound between $[-1, 1]$ unlike in PSO, it is limited between $[0, 1]$.

The proposed algorithm initially relies on the features of PSO to define the search area as well as on GWO to provide the best convergence. The HPSGWO algorithm finds the perfect solution with a suitability account for each search agent, updating the current search agent for each search agent. The coefficient vectors and inertia particles will then continue to be updated until the global optimum solution is obtained. Algorithm 1 shows the proposed algorithm:

Initialize *the GW population* $X_i\left(i = 1, 2, \ldots, N\right)$

Initialize A, and D

Calculate *the fitness of each search agent*

$\vec{X}_\alpha$ = *the best search agent*

$\vec{X}_\beta$ = *the best search agent*

$\vec{X}_\delta$ = *the best search agent*

while $(t < T_{max})$

　　For *each candidate solution*

　　　　Update *the position of the current search agent by equations 8, 9, and* 19

　　end for

　　Update A, and D *using equation 9 and* 20

　　Calculate *the fitness of all search agents.*

Update $\vec{X}_\alpha$, $\vec{X}_\beta$, *and* $\vec{X}_\delta$

t = t+1

end while

Return *the best solution obtained so far as the global optimum*

---

4 Experiments and results

In this section, we will perform a series of mono and multi-modal images registrations process to demonstrate the effectiveness of the new algorithm HPSGWO. The first stage of this section describes the image dataset we used in the registrations process. In the second stage, the results of the registration processes obtained after applying the proposed algorithm are presented and compared with the results of the PSO, GWO, FA, and CSA algorithms. All results of registration are obtained using the MATLAB R2020, on a computer having an Intel (R) Xeon (R) Silver 4108 GPU @1.80 GHz.

4.1 Image dataset

The test images used in this paper were obtained from the famous database "Radiopaedia" https://radiopaedia.org/articles/covid-19-4 , which provides modern CT images of the lungs of people infected with COVID-19 of all ages. Four types of computed tomography images are taken which are considered: The first CT image is denoted to as (CT-I1), the second image is CT-I2, the third image is (CT-I3), and the fourth image is (CT-I4).

4.2 Registration evaluation metrics

Several criteria have been proposed for evaluating image recording with the aim of showing the difference between the performances of different methods. In this paper, the Normalized Mutual Information (NMI), structural similarity (SSIM), and Human perception-based metric Q_{CB}, are used as quantitative evaluation measures to compare different recording algorithms. These criteria are simple and most used to evaluate the performance of various image-processing methods, and they are defined in order as follows:

- **Normalized Mutual Information (NMI)**
  The metric NMI is robust to change overlapping tissue regions, as it relies on a Parzen-window approach to estimate the probability density function [39]. For images A and B, the NMI is given as follows:

$$\text{NMI}(A, B) = \frac{H(A) + H(B)}{H(A, B)} \tag{21}$$

- **Structural SImilarity Metric (SSIM)**
  SSIM basically compares the standard image and the image to be detected from three aspects: Brightness, Contrast, and Structure Similarity [42].

$$\text{SSIM}\left(I_g, I_{s\_reg}\right) = \frac{\left(2\mu_g \mu_{s\_reg} + (k_1 L)^2\right)\left(2\sigma_{gs\_reg} + (k_2 L)^2\right)}{\left(\mu_g^2 + \mu_{s\_reg}^2 + (k_1 L)^2\right)\left(\sigma_g^2 + \sigma_{s\_reg}^2 + (k_2 L)^2\right)} \tag{22}$$

Where μ_g, μ_{s_reg}, σ_g, and σ_{s_reg} are the local means, standard deviations, and cross-covariance for images I_g, I_{s_reg}. k_1, k_2 are parameters with small values and L is the maximum pixel value.

- **Human perception-based metric (Q_{CB})**

     By the model of the human visual system, Chen and Blum [12] suggested a human perception-based metric Q_{CB}, which compares the features in the source image with those of the registered image. The measurement can be given as follows:

     The first step is to calculate the Q_{GQM} Global Quality Map by:

$$Q_{GQM} = \lambda_A(Q_{AF}(i, j)) + \lambda_B(Q_{BF}(i, j)) \qquad (23)$$

Where Q_{AR} (i, j) and Q_{BR}(i, j) represent the contrast in Q_{BR}(i, j) formation that was transferred from the source images A and B to the registered image R, respectively. λ_A and λ_B denote the saliency maps of Q_{AF} and Q_{BF} respectively. Q_{CB} can be calculated based on Q_{GQM} as shown in Eq. 26:

$$Q_{CB} = \overline{Q_{GQM}} \qquad (24)$$

A higher Q_{CB} value indicates that the registered image will retain more contrast information from the source images.

4.3 Accuracy of the registration process

In the experiments, the obtained of floating images by applying the following: translation $(t_x, t_y) = (7, 7)$ rotation of $\theta = 5°$ to the ground truth image, and similar population size of 25 and a maximum iteration value of 100 iterations to registred each pair of images.

     To confirm the effectiveness of the proposed algorithm and to clarify its performance in the image registration process and demonstrate the superiority of the proposed algorithm over the source algorithms, we applied the algorithms PSO and GWO separately on real 2D CT image pairs CT-I1, CT-I2, CT-I3, and CT-I4. These two algorithms have shown good results in registring pairs of magnetic resonance imaging (MRI) and computed tomography (CT) images in a previous study in [16]. On the other hand, due to the good results achieved by the FA and CSA algorithms in many optimization problems such as [3, 4, 7, 21, 25] respectively, these two algorithms were applied and the results obtained were compared with the results of the proposed algorithm. The algorithms were applied to a pair of "CT-I1" and "CT-I2" images of a lung infected to COVID-19 as a mono-modal, and the two pairs of "CT-I1 and CT-I2", "CT-I3 and CT-I4" as multi-modal.

     In the first stage of this experiment we considered the two pairs of CT images as mono-modal ((CT-I1, CT-I1) and (CT-I2, CT-I2)). The simulation results showed that the proposed algorithm HPSGWO is faster and more accurate in mono-modal registration of the two images pairs compared to the PSO, GWO, FA, and CSA algorithms. Tables 1 shows the registration parameters for the SSIM, NMI, and Q_{CB},

Table 1 Results for mono-modality registration

dataset 1

Moda-lities	CT-I1/CT-I1					CT-I3/CT-I3				
Algorithms	HPSGWO	PSO	GWO	FA	CSA	HPSGWO	PSO	GWO	FA	CSA
-t_x	**7.000412**	7.001985	7.019123	6.993805	6.960549	**6,997,868**	7.002332	7.024026	6.996462	7.003539
moy	**0,000412**	0,001985	0,019123	0,006195	0,039451	**0,002132**	0,002332	0,024026	0,003538	0,003539
-t_y	6.999678	6.999129	7.006428	**7.000042**	7.013669	**7,000,189**	6.999760	6.967417	7.004477	6.999533
moy	0,000322	0,000871	0,006428	**0,000042**	0,013669	**0,000189**	0,00024	0,032583	0,004477	0,000467
-θ	**5,000352**	4.99884	4.999178	4.997836	4.993334	**5,000,348**	4.999471	4.994060	4.997552	4.999305
moy	**0,000352**	0,00116	0,000822	0,002164	0,006666	**0,000348**	0,000529	0,00594	0,002448	0,000695
SSIM	**0.999997**	0.999965	0.999966	0.999992	0.999929	**0.999991**	0.999963	0.999961	0.999992	0.999926
NMI	**1.292493**	1.292471	1.292492	1.291718	1.278372	**1.29421**	1.294632	1.294999	1.295024	1.294632
Q_{CB}	**0.695892**	0.6782924	0.677178	0.678692	0.677873	**0.680009**	0.666567	0.6632807	0.670559	0.66090
Time (S)	**42.94527**	78.36011	48.23693	568.5125	49.00174	**38.21095**	68.75508	45.64086	506.8556	46.98393
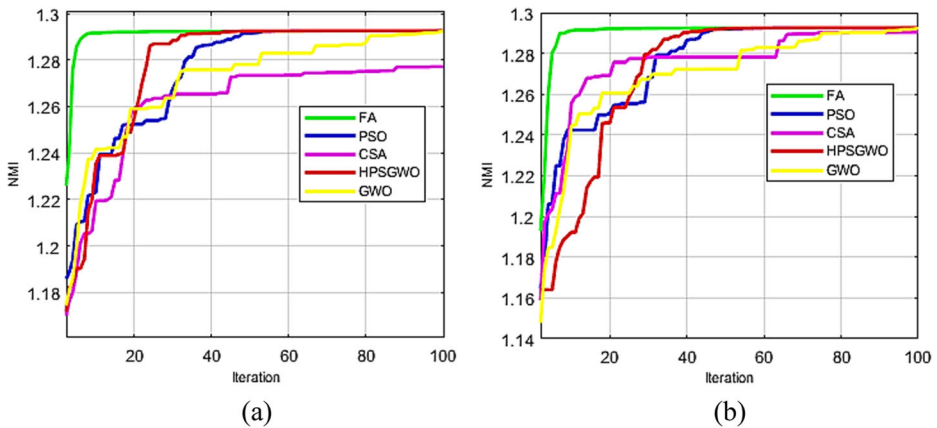
Fig. 5 Convergence curves for the algorithms used resulting from mono-modal registration of CT images: (a) CT-I1/CT-I1 and (b) CT-I3/CT-I3

values for each pair of images. It clearly shows that the proposed algorithm has found the optimal solutions to the registration process and within a short period on all tests over 20 runs. The maximum SSIM, INM, and Q_{CB} values in the proposed algorithm appear in both registration. Figure 8 shows the percentages of the algorithms used based on SSIM, which further illustrate the superiority of the proposed algorithm for mono-modal registration of the two image pairs.

Through Fig. 5 showing the evolution of the algorithms used in this experiment (for mono-modal registration), it can be seen that the proposed algorithm HPSGWO and the FA algorithm converge after 45 and 5 iterations, respectively, for the image pairs ((CT-I1,CT-I1) and (CT-I3,CT-I3)). While other algorithms need more than 60 iterations to converge. Despite the high evaluation values of the proposed method compared to other methods, which indicate better registration results, they converge after a large number of iterations compared to FA, which converge after a very small number of iterations. This is due to the reduction in the search area, and to get closer to the optimal solution to obtain the best results of registration.

The visual quality of different mono-modal image registration methods (HPSGWO, PSO, FA, CSA, and GWO) is presented in two Figs. 6 and 7. these results confirm the good performance of the proposed HPSGWO algorithm, as it contains higher SSIM, INM, and Q_{CB} values, that indicating better mono-modal registration results. The green and magenta color distribution show the information of the source image and sensed image, respectively. The difference between images before registration and Registered image confirms the recording effectiveness of the algorithms in general and the proposed algorithm in particular.

•   A-frame has been added to the SSIM Map images to show their borders only, this frame does not belong to the resulting images.

In the second stage of this experiment, we considered the two pairs of CT images as multi-modal ((CT-I1, CT-I2) and (CT-I3, CT-I4)). The simulation results showed that the proposed
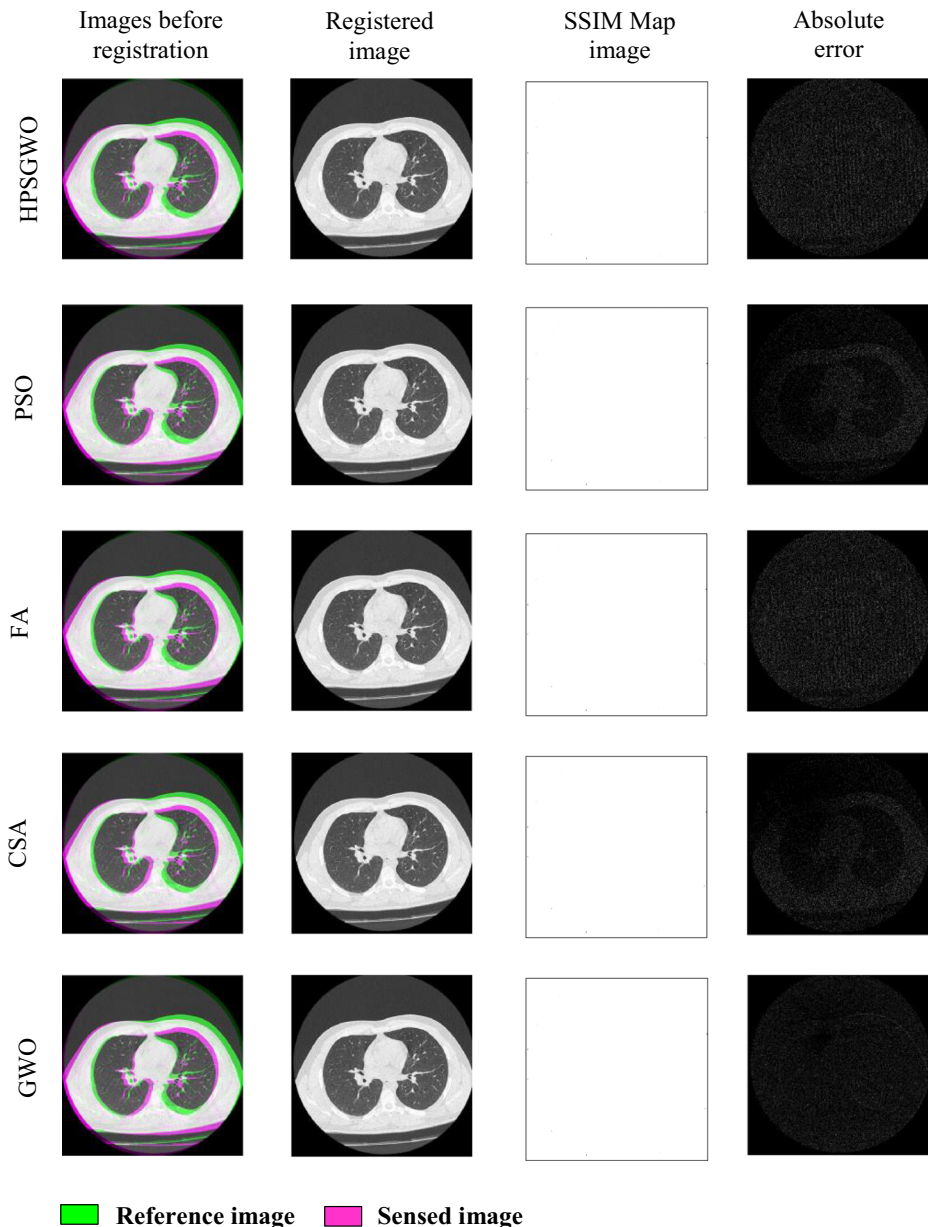
Fig. 6 Visual results obtained from mono-modal image registration of pair (CT-I1/CT-I1) using the HPSGWO algorithm: (a) Images before registration, (b) Registered image, (c) SSIM Map image, and (d) Absolute error

algorithm HPSGWO is faster and more accurate in multi-modal registration of the two images pairs compared to the PSO, GWO, FA, and CSA algorithms. Tables 2 shows the registration parameters for the SSIM, INM, and Q_{CB} values for each pair of images. It clearly shows that the proposed algorithm has found the optimal solutions to the registration process and within a short period on all tests over 20 runs as it happened in mono-modal registration in the first
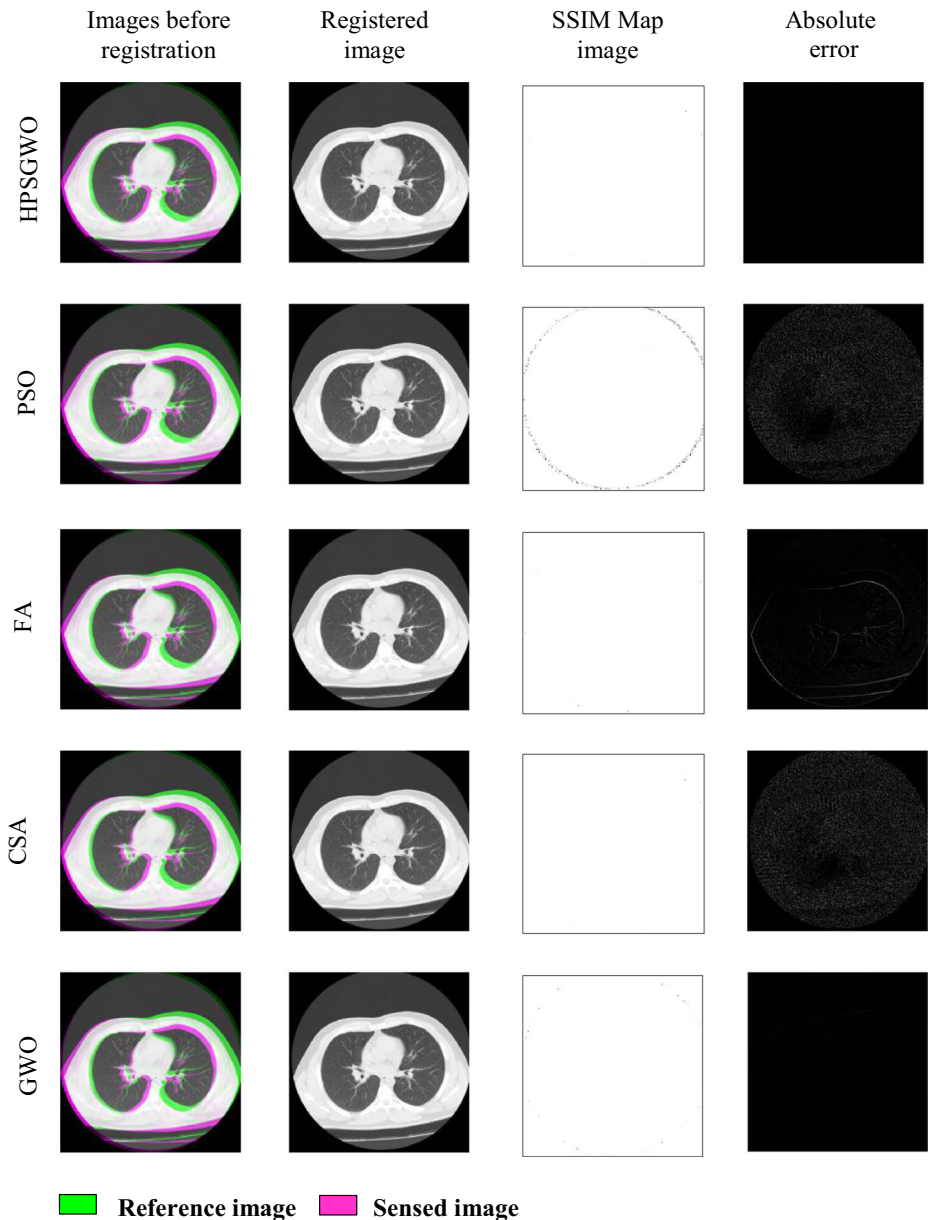
Fig. 7 Visual results obtained from mono-modal image registration of pair (CT-I3/CT-I3) using the HPSGWO algorithm: (a) Images before registration, (b) Registered image, (c) SSIM Map image, and (d) Absolute error

stage. Figure 8 shows the relative percentages of the algorithms used based on SSIM, which further illustrate the superiority of the proposed algorithm for the two multi-modal image pairs registration.

Through Fig. 9 showing the evolution of the algorithms used in this experiment, it can be seen that the proposed algorithm HPSGWO and the FA algorithm converge after 45 and 5 iterations, respectively, for the image pairs ((CT-I1,CT-I2) and (CT-I3,CT-I4)) as it

Table 2 Results for multi-modality registration

dataset 1

Moda-lities	CT-I1/CT-I2					CT-I3/CT-I4				
Algorithms	HPSGWO	PSO	GWO	FA	CSA	HPSGWO	PSO	GWO	FA	CSA
$-t_x$	**6.998905**	7.002326	6.994191	6.995947	7.001162	**70,001,231**	7.007505	7.031315	7.009575	7.007565
moy	**0,001095**	0,002326	0,005809	0,004053	0,001162	**0,000123**	0,007505	0,031315	0,009575	0,007565
$-t_y$	**6,999.758**	6.999748	6.993237	7.005332	6.999105	**6,983,549**	7.026365	7.032691	7.024802	7.027856
moy	**0,000242**	0,000252	0,006763	0,005332	0,000895	**0,016451**	0,026365	0,032691	0,024802	0,027856
$-\theta$	4,988,744	**4.999480**	5.002055	4.998162	4.999316	4.974629	4.997856	4.995340	4.996741	**4.998678**
moy	0,011256	**0,00052**	0,002055	0,001838	0,000684	0,025371	0,002144	0,004660	0,003259	**0,001322**
SSIM	**0.999996**	0.999963	0.999975	0.999994	0.999919	**0.999967**	0.999960	0.999964	0.999961	0.999930
NMI	**1.285034**	1.284839	1.285023	1.283494	1.285007	**1.164344**	1.163759	1.163757	1.163760	1.163728
Q_{CB}	**0.679505**	0.664896	0.674893	0.6646126	0.645959	**0.681419**	0.670957	0.670544	0.671555	0.651017
Time (S)	**32.77379**	46.52661	42.42466	514.6154	73.65165	**41.21114**	43.84314	41.81606	556.78873	64.29531
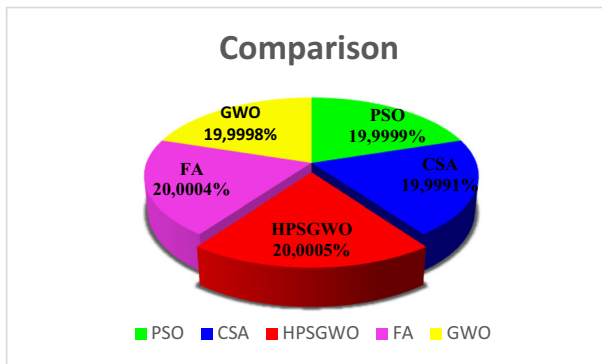
Fig. 8 Mono-modal images Registration accuracy comparison of HPSGWO, PSO, GWO, FA, and CSA algorithms based on SSIM

happened in mono-modal registration in the first stage. While other algorithms need more than 60 iterations to converge. As is the case in mono-modal registration, despite the high SSIM, INM, and Q_{CB} values shown in the proposed method, they converge after a very large number of iterations compared to the FA algorithm. This is due to the reduction in the search area, and to get closer to the optimal solution to obtain the best results of registration.

The visual quality of different multi-modal image registration methods (HPSGWO, PSO, FA, CSA, and GWO) is presented in two Figs. 10 and 11. These results confirm the good performance of the proposed HPSGWO algorithm, as it contains higher SSIM, INM, and Q_{CB} values, that indicating better multi-modal registration results. The green and magenta color distribution show the information of the source image and sensed image, respectively. The difference between images before registration and Registered image confirms the recording effectiveness of the algorithms in general and the proposed algorithm in particular.

- A-frame has been added to the SSIM Map images to show their borders only, this frame does not belong to the resulting images.
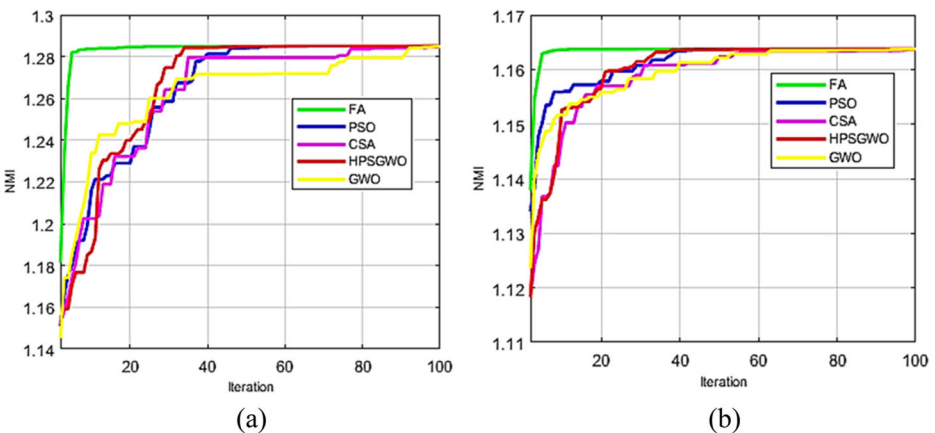
Fig. 9 Convergence curves for the algorithms used resulting from multi-modal registration of CT images: (a) CT-I3/CT-I4 and (b) CT-I1/CT-I2

	Images before registration	Registered image	SSIM Map image	Absolute error
HPSGWO				
PSO				
FA				
CSA				
GWO				

🟩 **Reference image**   🟪 **Sensed image**
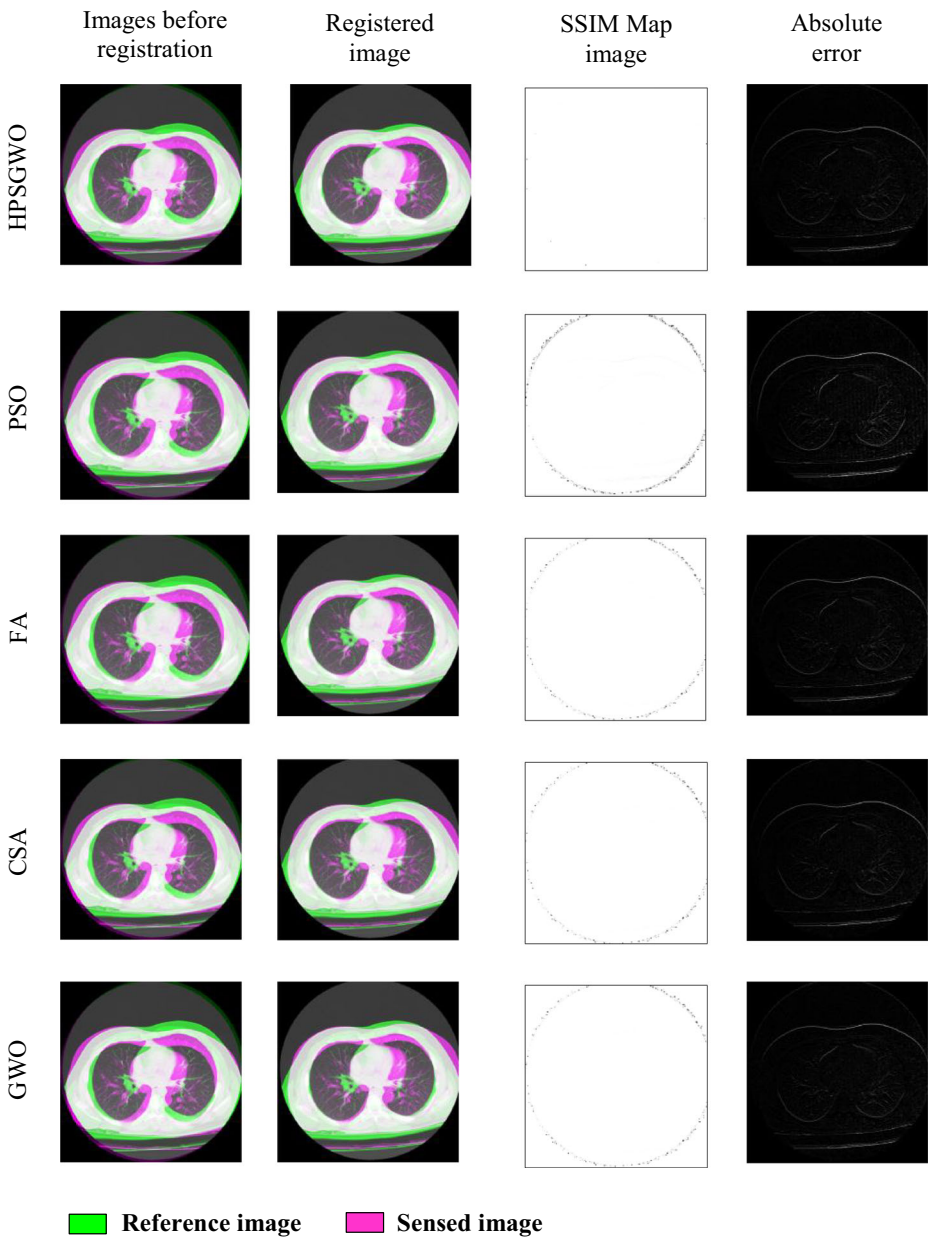
Fig. 10 Visual results obtained from multi-modal image registration of pair (CT-I3/CT-I4) using the HPSGWO algorithm: (a) Images before registration, (b) Registered image, (c) SSIM Map image, and (d) Absolute error

Figure 12 shows the percentages of the algorithms used based on SSIM, which further illustrate the superiority of the proposed algorithm for multi-modal registration of the two image pairs.
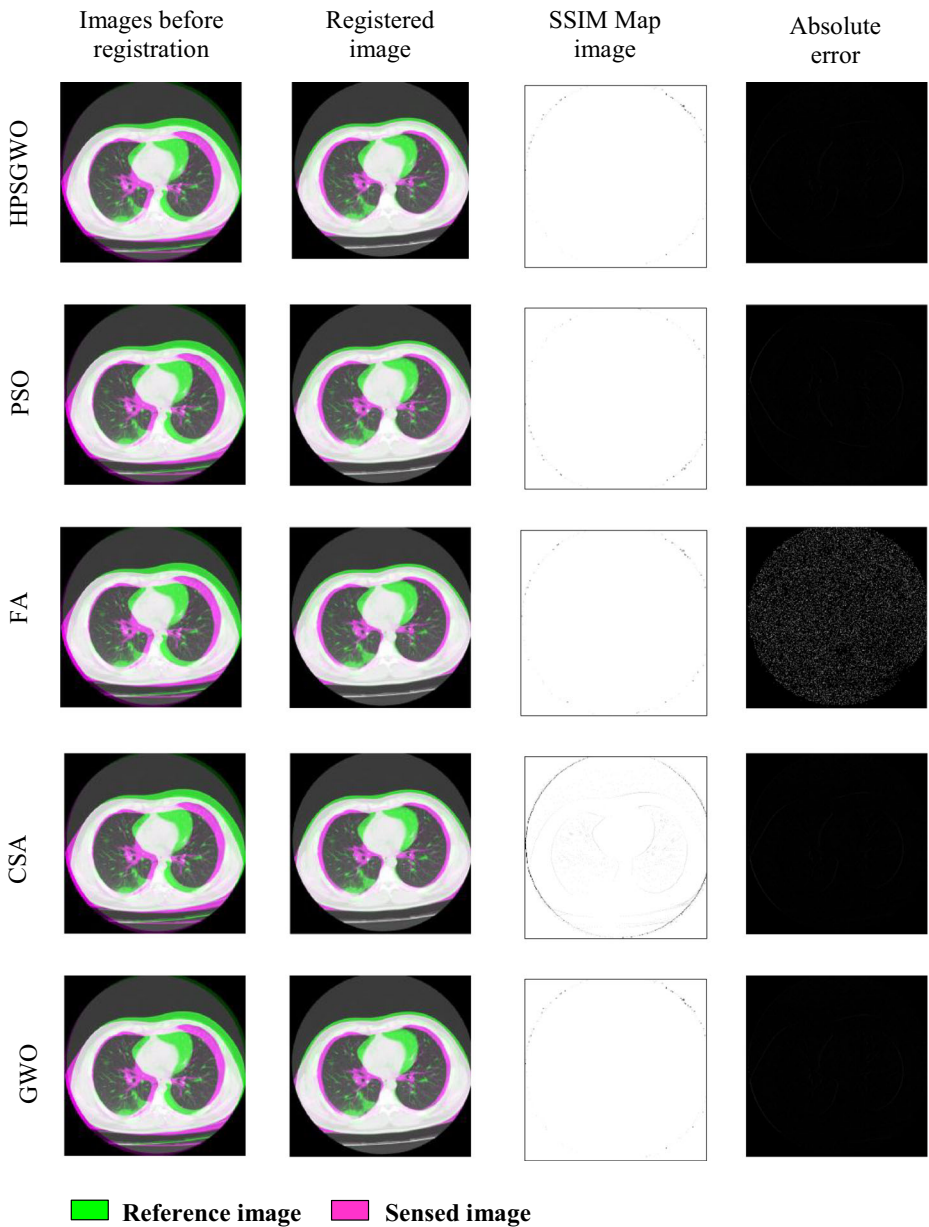
Fig. 11 Visual results obtained from multi-modal image registration of pair (CT-I1/CT-I2) using the HPSGWO algorithm: (a) Images before registration, (b) Registered image, (c) SSIM Map image, and (d) Absolute error

4.4 Comparisons with the latest deep learning methods

To confirm the good performance of the proposed method for rigid registration of CT images of people infected with COVID-19 and to generalize their use, we compared them on the basis of the structural similarity metric (SSIM), Normalized Mutual
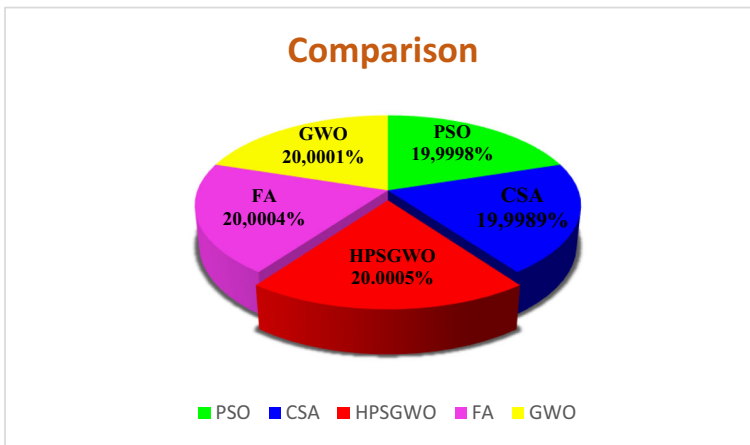
Fig. 12 Multi-modal images Registration accuracy comparison of HPSGWO, PSO, GWO, FA, and CSA algorithms based on SSIM

Information (NMI), Human perception-based metric Q_{CB} and with the available method of registration based in deep learning. The same database used for deep learning-based registration was implemented in [33]. The following table shows the results obtained, to show the good performance of the proposed method. The following table shows the results obtained, that shows the superiority of the proposed method in the registration process (Table 3).

5 Conclusion

In this work, we used a new method resulting from the hybridization of two well-known algorithms PSO and GWO (named HPSGWO) to registered CT images of lung infected with COVID-19 that contain GGO. First, HPSGWO, PSO, GWO, FA, and CSA algorithms were used for mono-modal registration and then used for multi-modal registration of CT images of lung infected with COVID-19. The results obtained showed that the proposed method achieves good recording and is superior to the PSO, GWO, FA, and CSA algorithms in most cases of multi-modal and mono-modal registration of the test images.

Table 3 A comparative study of the proposed method with an existing method based on deep learning (deep convolutional inverse graphics network)

Dataset2

Evaluaion	PSO	GWO	FA	CSA	DCIGN	Proposed method
SSIM	0.9997	0.9409	0.9996	0.9991	0.9700	**0.9998**
NMI	1.1843	1.1841	1.1843	1.1672	0.7400	**1.1844**
Q_{CB}	0.6689	0.6508	0.6508	0.6208	–	**0.6699**

References

1. Ahmed HA, Zolkipli MF, Ahmad M (2019) A novel efficient substitution-box design based on firefly algorithm and discrete chaotic map. Neural Comput Appl 31(11):7201–7210. https://doi.org/10.1007/s00521-018-3557-3
2. Altabeeb AM, Mohsen AM, Ghallab A (2019) An improved hybrid firefly algorithm for capacitated vehicle routing problem. Appl Soft Comput J 84:105728. https://doi.org/10.1016/j.asoc.2019.105728
3. Anter AM, Hassenian AE, Oliva D (2019) An improved fast fuzzy c-means using crow search optimization algorithm for crop identification in agricultural. Expert Syst Appl 118:340–354. https://doi.org/10.1016/j.eswa.2018.10.009
4. Ball AK, Roy SS, Kisku DR, Murmu NC, and Dos S. Coelho L (2020) Optimization of drop ejection frequency in EHD inkjet printing system using an improved Firefly Algorithm Appl. Soft Comput. J. 94: 106438 https://doi.org/10.1016/j.asoc.2020.106438.
5. Bashiri FS and Baghaie A (2019) Multi-Modal Medical Image Registration with Full or Partial Data: A Manifold Learning Approach. 12–17. https://doi.org/10.3390/jimaging5010005.
6. Bavirisetti DP, Kollu V, Gang X, Dhuli R (2017) Fusion of MRI and CT images using guided image filter and image statistics. Int J Imaging Syst Technol 27(3):227–237. https://doi.org/10.1002/ima.22228
7. Bennis F and Kumar R (2020) Nature-Inspired Methods for Metaheuristics Optimization. 16
8. Bozorg-Haddad O (2018) Studies in computational intelligence - advanced optimization by nature-inspired algorithms
9. Cai J (2020) Based on DPC and PSO. 8 https://doi.org/10.1109/ACCESS.2020.2992903.
10. Chen Y, … Chen W (2014) Artifact suppressed dictionary learning for low-dose CT image processing. IEEE Trans Med Imaging 33(12):2271–2292. https://doi.org/10.1109/TMI.2014.2336860
11. Chen Y, … Feng Q (2018) Structure-adaptive fuzzy estimation for random-valued impulse noise suppression. IEEE Trans Circuits Syst Video Technol 28(2):414–427. https://doi.org/10.1109/TCSVT.2016.2615444
12. Chen Y, Blum RS (2009) A new automated quality assessment algorithm for image fusion. Image Vis Comput 27(10):1421–1432. https://doi.org/10.1016/j.imavis.2007.12.002
13. Chen Y, He F, Li H, Zhang D, Wu Y (2020) A full migration BBO algorithm with enhanced population quality bounds for multimodal biomedical image registration. Appl Soft Comput J 93:106335. https://doi.org/10.1016/j.asoc.2020.106335
14. Chung M, … Shan H (2020) CT imaging features of 2019 novel coronavirus (2019-NCoV). Radiology 295(1):202–207. https://doi.org/10.1148/radiol.2020200230
15. David JVH, Hill DLG, Hawkes DJ (2001) Medical Image Registration. Biomedical engineering series. RC78.7.D53 M436
16. Dida H, Charif F, and Benchabane A (2020) Grey Wolf Optimizer for Multimodal Medical Image Registration. 4th Int. Conf. Intell. Comput. Data Sci. ICDS. 1: 0–4.https://doi.org/10.1109/ICDS50568.2020.9268771.
17. Dong J, Lu K, Xue J, Dai S, Zhai R, and Pan W (2018) Accelerated nonrigid image registration using improved Levenberg–Marquardt method. Inf. Sci. (Ny). 423: 66–79 https://doi.org/10.1016/j.ins.2017.09.059.
18. Du K-L and Swamy MNS (2016) Search and Optimization by Metaheuristics https://doi.org/10.1007/978-3-319-41192-7
19. Ferrante E, Paragios N (2017) Slice-to-volume medical image registration: a survey. Med Image Anal 39: 101–123. https://doi.org/10.1016/j.media.2017.04.010
20. Goshtasby AA (2003) 2-D and 3-D Image Registration. Wiley-Interscience publication. https://doi.org/10.16309/j.cnki.issn.1007-1776.03.004
21. Hussien AG, … Chen H (2020) Crow search algorithm: theory, recent advances, and applications. IEEE Access 8:173548–173565. https://doi.org/10.1109/access.2020.3024108
22. Kaveh A, Bakhshpoori T (2019) Metaheuristics: outlinesMATLAB Codes and Examples. https://doi.org/10.1007/978-3-030-04067-3
23. Khalilpourazari S, Pasandideh SHR (2020) Sine–cosine crow search algorithm: theory and applications. Neural Comput Appl 32(12):7725–7742. https://doi.org/10.1007/s00521-019-04530-0
24. Li Y, Xia L (2020) Coronavirus disease 2019 (COVID-19): role of chest CT in diagnosis and management. Am J Roentgenol 214(6):1280–1286. https://doi.org/10.2214/AJR.20.22954
25. Majhi SK, Sahoo M, Pradhan R (2020) A space transformational crow search algorithm for optimization problems. Evol Intell 13(3):345–364. https://doi.org/10.1007/s12065-019-00294-7
26. Mungmungpuntipantip R and Wiwanitkit V (2020) Clinical Features and Chest CT Manifestations of Coronavirus Disease (COVID-19). AJR. Am. J. Roentgenol. 215(1): W13. https://doi.org/10.2214/AJR.20.23141.

27. Ozdemir G, Karaboga N (2019) A review on the cosine modulated filter bank studies using meta-heuristic optimization algorithms. Artif Intell Rev 52(3):1629–1653. https://doi.org/10.1007/s10462-017-9595-x

28. Prithi S, Sumathi S (2021) Automata based hybrid PSO–GWO algorithm for secured energy efficient optimal routing in wireless sensor network. Wirel Pers Commun 117(2):545–559. https://doi.org/10.1007/s11277-020-07882-2

29. Saha SK, Xiao D, Bhuiyan A, Wong TY, Kanagasingam Y (2019) Color fundus image registration techniques and applications for automated analysis of diabetic retinopathy progression: a review. Biomed Signal Process Control 47:288–302. https://doi.org/10.1016/j.bspc.2018.08.034

30. Şenel FA, Gökçe F, Yüksel AS, Yiğit T (2019) A novel hybrid PSO–GWO algorithm for optimization problems. Eng Comput 35(4):1359–1373. https://doi.org/10.1007/s00366-018-0668-5

31. Shekhawat S and Saxena A (2020) Development and applications of an intelligent crow search algorithm based on opposition based learning. ISA Trans.99(xxxx): 210–230 https://doi.org/10.1016/j.isatra.2019.09.004.

32. Tu Q, Chen X, Liu X (2019) Multi-strategy ensemble grey wolf optimizer and its application to feature selection. Appl. Soft Comput. J. 76:16–30. https://doi.org/10.1016/j.asoc.2018.11.047

33. Vasant J et al (2018) An unsupervised convolutional neural network-based algorithm for deformable image registration. Phys Med Biol 63(18):185017

34. Wang D, Tan D, Liu L (2018) Particle swarm optimization algorithm: an overview. Soft Comput 22(2):387–408. https://doi.org/10.1007/s00500-016-2474-6

35. Wang F, Zhang H, Zhou A (2021) A particle swarm optimization algorithm for mixed-variable optimization problems. Swarm Evol Comput 60:100808. https://doi.org/10.1016/j.swevo.2020.100808

36. Wang M, Li P (2019) A Review of Deformation Models in Medical Image Registration. J. Med. Biol. Eng. 39(1). https://doi.org/10.1007/s40846-018-0390-1

37. Wang WC, Xu L, Chau KW, Xu DM (2020) Yin-Yang firefly algorithm based on dimensionally Cauchy mutation. Expert Syst. Appl. 150:113216. https://doi.org/10.1016/j.eswa.2020.113216

38. Wu J, Wang YG, Burrage K, Tian YC, Lawson B, Ding Z (2020) An improved firefly algorithm for global continuous optimization problems. Expert Syst Appl 149:113340. https://doi.org/10.1016/j.eswa.2020.113340

39. Wu S, He P, Yu S, Zhou S, Xia J, and Xie Y (2020) "To Align Multimodal Lumbar Spine Images via Bending Energy Constrained Normalized Mutual Information. 2020

40. Yin X, … Luo L (2019) Domain progressive 3D residual convolution network to improve low-dose CT imaging. IEEE Trans Med Imaging 38(12):2903–2913. https://doi.org/10.1109/TMI.2019.2917258

41. Yin Z, Kang Z, Yang D, Ding S, Luo H, and Xiao E (2020) "A Comparison of Clinical and Chest CT Findings in Patients With Influenza A (H1N1) Virus Infection and Coronavirus Disease (COVID-19)," Am. J. Roentgenol. 1–7. https://doi.org/10.2214/ajr.20.23214.

42. Zhou M, Wang G, Wang J, Hui C, and Yang W (2017) Defect Detection of Printing Images on Cans Based on SSIM and Chromatism. 1–5